# Membrane potential independent transport of $NH_3$ in the absence of ammonium permeases in Saccharomyces cerevisiae

Cueto-Rojas, Hugo F.; Milne, Nicholas; van Helmond, Ward; Pieterse, Mervin M.; Maris, Antonius J A; Daran, Jean Marc; Wahl, S. Aljoscha

**DOI**
10.1186/s12918-016-0381-1

**Publication date**
2017

**Document Version**
Final published version

**Published in**
BMC Systems Biology

Cueto-Rojas et al. BMC Systems Biology (2017) 11:49
DOI 10.1186/s12918-016-0381-1

BMC Systems Biology

RESEARCH ARTICLE Open Access

# Membrane potential independent transport of $NH_3$ in the absence of ammonium permeases in *Saccharomyces cerevisiae*

Hugo F. Cueto-Rojas[1†], Nicholas Milne[1,2†], Ward van Helmond[1,3], Mervin M. Pieterse[1], Antonius J. A. van Maris[1,4], Jean-Marc Daran[1*] and S. Aljoscha Wahl[1*]

## Abstract

**Background:** Microbial production of nitrogen containing compounds requires a high uptake flux and assimilation of the N-source (commonly ammonium), which is generally coupled with ATP consumption and negatively influences the product yield. In the industrial workhorse *Saccharomyces cerevisiae*, ammonium ($NH_4^+$) uptake is facilitated by ammonium permeases (Mep1, Mep2 and Mep3), which transport the $NH_4^+$ ion, resulting in ATP expenditure to maintain the intracellular charge balance and pH by proton export using the plasma membrane-bound $H^+$-ATPase.

**Results:** To decrease the ATP costs for nitrogen assimilation, the Mep genes were removed, resulting in a strain unable to uptake the $NH_4^+$ ion. Subsequent analysis revealed that growth of this Δ*mep* strain was dependent on the extracellular $NH_3$ concentrations. Metabolomic analysis revealed a significantly higher intracellular $NH_X$ concentration (3.3-fold) in the Δ*mep* strain than in the reference strain. Further proteomic analysis revealed significant up-regulation of vacuolar proteases and genes involved in various stress responses.

**Conclusions:** Our results suggest that the uncharged species, $NH_3$, is able to diffuse into the cell. The measured intracellular/extracellular $NH_X$ ratios under aerobic nitrogen-limiting conditions were consistent with this hypothesis when $NH_x$ compartmentalization was considered. On the other hand, proteomic analysis indicated a more pronounced N-starvation stress response in the Δ*mep* strain than in the reference strain, which suggests that the lower biomass yield of the Δ*mep* strain was related to higher turnover rates of biomass components.

**Keywords:** Intracellular ammonium, Metabolomics, Ammonium transport, Central nitrogen metabolism, Ammonia passive diffusion, Thermodynamics

## Background

A significant number of fuels and commodity chemicals have the potential to be produced in bio-refineries using microbial fermentation, which represents a more sustainable alternative to current oil-based production [1]. The increasing interest in microbial-based production is best exemplified by the intensive research efforts to improve the productivity and yield of a vast range of different compounds produced by *Saccharomyces cerevisiae* [2, 3] and other industrial workhorses. Nevertheless, while the number of compounds produced at industrial scale by *S. cerevisiae* is increasing, the production of nitrogen-containing compounds using *S. cerevisiae* is significantly under-represented, with heterologous protein production being the only known example [3].

Nitrogen-containing compounds represent an economically relevant class of commodity chemicals that includes amino acids such as L-lysine and L-glutamate, diamines such as 1,5-diaminopentane (cadaverine) and 1,4-diaminobutane (putrescine), and relevant synthesis precursors such as caprolactam. Their microbial production is currently performed under aerobic conditions using bacteria, most commonly *Corynebacterium glutamicum* and *Escherichia coli* [4–6].

* Correspondence: J.G.Daran@tudelft.nl; S.A.Wahl@tudelft.nl
†Equal contributors
[1]Department of Biotechnology, Delft University of Technology, van der Maasweg 9, 2629HZ Delft, The Netherlands
Full list of author information is available at the end of the article

Along with bacteria, *S. cerevisiae* is seen as an attractive host organism for industrial fermentation due to its fast anaerobic conversion of sugar to product, its resistance to phage attack, and its robustness under common industrial conditions [7]. When using *S. cerevisiae* for the production of nitrogen-containing compounds, the process should preferably occur under anaerobic conditions [8] if this is permitted by the thermodynamics and biochemistry of the product pathway. Anaerobic conditions are favorable not only in terms of the resulting fermentation costs, but also in terms of the product yield [9]. Under such conditions, however, the energy supply relies solely on substrate-level phosphorylation, limiting the amount of ATP available for growth and maintenance. Consequently, the anaerobic production of nitrogen-containing compounds should result in net ATP formation and it is essential that the N-source be transported and assimilated using ATP-independent mechanisms.

Urea and ammonium are the most common N-sources used industrially in *S. cerevisiae* fermentations. Previously, we presented a novel strategy for achieving ATP-independent urea assimilation in *S. cerevisiae* [10]. While urea is an attractive nitrogen source, ammonium is more commonly used in industrial fermentation and is also present in plant hydrolysates used for second-generation chemical production [11, 12]. Mechanisms for ATP-neutral ammonium transport and assimilation would have significant relevance for the anaerobic production of nitrogen-containing compounds. Ammonia ($NH_3$) protonates in aqueous solutions to produce the ammonium ion ($NH_4^+$), the sum of these two species, $NH_3$ and $NH_4^+$, will be described henceforth as $NH_X$. With a *pKa* of 9.25, under biologically relevant conditions (between pH 3 and 7), the ratio $NH_3/NH_4^+$ equals $10^{pH-9.25}$, meaning that the vast majority of the $NH_X$ is present as the charged ammonium species ($NH_4^+$).

In *S. cerevisiae*, $NH_4^+$ is taken up by the ammonium permeases Mep1, Mep2, and Mep3, which belong to the Amt class of proteins that use the negative membrane potential as their thermodynamic driving force [13]. The evolutionary advantage of this transport mechanism, compared with passive diffusion, is a higher transport rate. And, due to the negative cytosolic membrane potential, accumulation of intracellular $NH_X$ is favored. However, one $H^+$ must be exported from the cytosol by the plasma-membrane-bound $H^+$-ATPase Pma1 [14] to recover the proton motive force (pmf) and charge homeostasis after $NH_4^+$ import, and subsequent assimilation of $NH_3$ [8]. The deletion of the ammonium permease genes Mep1, Mep2, and Mep3 results in a viable strain able to grow on ammonium concentrations above 5 mM. Previously, it has been assumed that there are additional ammonium transporters [15] or that there is non-specific transport through potassium channels [16]. However, we here present an alternative hypothesis: that the uncharged $NH_3$ species can diffuse into the cell. If this were correct, it would result in ATP-independent $NH_X$ uptake and consequently reduce the demand for ATP demand. Previous experimental observations in synthetic bilayer lipid membranes suggest that the $NH_3$ apparent permeability coefficient is $P_{1a} = 1.728$ m/h ($48 \times 10^{-3}$ cm/s) [17], which indicates that cell membranes are indeed permeable to $NH_3$.

Here, we study the $NH_X$-uptake mechanism in a Δ*mep S. cerevisiae* strain, and assess the impact of the deletion of Mep1, Mep2, and Mep3 on the physiology of *S. cerevisiae*. Proteomic and metabolomic measurements are used to investigate the global impact of the changed $NH_X$-uptake mechanism on cellular physiology.

## Methods

### Strains and maintenance

All *Saccharomyces cerevisiae* strains used in this study (Table 1) were derived from the CEN.PK strain family background [18, 19], details about strain contraction are found in Additional file 1. Frozen stocks of *E. coli* and *S. cerevisiae* were prepared by addition of glycerol (30% (v/v)) to exponentially growing cells followed by aseptic storage of 1 mL aliquots at -80 °C. Cultures were grown at 30 °C either in synthetic medium [20] with 20 g/L glucose as carbon source and appropriate growth factors [21], or complex medium containing 20 g/L glucose, 10 g/L Bacto yeast extract and 20 g/L Bacto peptone. If required for anaerobic growth Tween-80 (420 mg/L) and ergosterol (10 mg/L) were added. Agar plates were prepared as described above but with the addition of 20 g/L agar (Becton Dickinson B.V. Breda, The Netherlands).

### Strain cultivation

#### *Shake flask cultivation*

*S. cerevisiae* strains were grown in synthetic medium [22]. Cultures were grown in either 500 mL or 250 mL shake flasks containing 100 mL or 50 mL of medium, respectively, and incubated at 30 °C in an Innova incubator shaker (New Brunswick Scientific, Edison, NJ) at 200 rpm.

#### *Aerobic nitrogen-limited chemostat cultivation*

Controlled aerobic, nitrogen limited chemostat cultivations were carried out at 30 °C in 7 L bioreactors (Applikon Biotechnology B.V., Delft, the Netherlands) with a working volume of 4 L. Chemostat cultivations were preceded by a batch phase using the same synthetic medium as used for the feed. Continuous cultivation was initiated at a dilution rate of 0.05 $h^{-1}$; synthetic nitrogen-limited medium was used modified from [23], which contained: 130 g/L glucose, 25 g/L ethanol, 3.48 g/L $NH_4H_2PO_4$, 1.14 g/L $MgSO_4 \cdot 7H_2O$, 6.9 g/L $KH_2PO_4$, 0.3 g/L Antifoam C, with the

**Table 1** Strains used in this study

| Name | Relevent genotype | Origin |
|---|---|---|
| CEN.PK113-3B | *MATalpha ura3-52 his3-D1 LEU2 TRP1 MAL2-8c SUC2* | [18] |
| CEN.PK113-3B-Δmep1 | *MATalpha ura3-52 his3-D1 LEU2 TRP1 MAL2-8c SUC2 mep1::loxP*-KanMX4-loxP | This study |
| CEN.PK113-3B-Δmep1, Δmep 2 | *MATalpha ura3-52 his3-D1 LEU2 TRP1 MAL2-8c SUC2 mep1::loxP*-KanMX4-*loxP mep2::loxP*-NatNT2-*loxP* | This study |
| CEN.PK113-3B-Δmep1, Δmep 2, Δmep 3 | MATalpha ura3-52 his3-D1 LEU2 TRP1 MAL2-8c SUC2 *mep1::loxP*-KanMX4-*loxP mep2::loxP*-NatNT2-loxP *mep3::loxP-Ura3-loxP* | This study |
| CEN.PK113-3B-Δmep1, Δmep 2, Δmep 3-Cure | *MATalpha ura3-52 his3-D1 LEU2 TRP1 MAL2-8c SUC2 mep1::loxP-loxP mep2::loxP-loxP mep3::loxP-loxP* | This study |
| IMZ351 | *MATalpha ura3-52 his3-D1 LEU2 TRP1 MAL2-8c SUC2 mep1::loxP-loxP mep2::loxP-loxP mep3::loxP-loxP* pUDE199 (*HIS3 URA3*) | This study |
| IME169 | *MATalpha ura3-52 his3-Δ1 LEU2 TRP1 MAL2-8c SUC2* pUDE199 (*HIS3 URA3*) | This study |

appropriate growth factors added accordingly [21] (vitamin solution 2 mL/L and trace element solution 2 mL/L), ethanol was added to the medium to avoid potential oscillations. The medium was designed to sustain a biomass concentration of up to 8 g/L in nitrogen-limited anaerobic conditions for the wild type (CEN.PK113-7D) strain. The temperature and stirring speed were kept constant at 30 °C and 500 rpm, respectively. The reactor had an overpressure of 0.3 bar, and an aeration rate of 0.5 vvm was used to keep the dissolved oxygen level above 80%. Dissolved oxygen tension (DOT) was monitored online using an oxygen probe (Mettler-Toledo, Tiel, The Netherlands), and a combined paramagnetic/infrared analyser (NGA 2000, Fisher-Rosemount, Hasselroth, Germany) was used to measure $CO_2$ and $O_2$ fractions in the off-gas. During the batch phase and the first steady state the pH was kept constant at a value of 5 with automatic additions of 4 M KOH or 2 M $H_2SO_4$; after reaching steady state and sampling, the pH control was changed to maintain a constant value of 6, while keeping the dilution rate constant; the same operation was performed for the switch from pH = 6 to pH = 7. All samples were taken at steady state between three and seven volume changes after switching on the medium addition or pH changes.

## Sampling and sample preparation

### *Extracellular sampling*

For aerobic nitrogen limited chemostats, samples of approx. 2 mL were quenched using cold steel beads [24], and filtered using 0.45 μm disc filters (Milipore). Samples for residual ammonium determination were prepared by mixing 80 μL of sample with 20 μL of internal standard (500 μmol/L $^{15}N$-$NH_4Cl$) and quantified according to [25]. All samples were stored at -80 °C until further analysis.

### *Intracellular sampling*

Samples containing approximately 1.2 g broth were obtained using a dedicated setup, as described by [26], quenched in 6 mL of -40 °C methanol 100%, and after weighing to accurately determining the mass of each sample, these were centrifuged for 5 min at 10,000 g and -19 °C. The pellet was recovered and resuspended in 6 mL -40 °C methanol 100%; then centrifuged again for 5 min at 10,000 g and -19 °C [27].

### *Intracellular ammonium extraction*

The biomass pellet obtained from *Intracellular sampling* was recovered, 3.5 mL of Methanol-acetate buffer 10 mM (pH = 5) 50%(v/v) pre-chilled at -40 °C was added, and then 120 μL of U-$^{13}C$- cell extract with labeled urea (intracellular metabolites samples) or 120 μL of $^{15}N$- $NH_4Cl$ 500 μmol/L (intracellular ammonium samples) were added as internal standard. Afterwards, 3.5 mL of Chloroform 100% pre-chilled at -40 °C was added in order to extract intracellular metabolites according to [25]. Samples for quantification of intracellular ammonium were extracted using exclusively this method.

### *Intracellular metabolite extraction*

The biomass pellet (*Intracellular sampling*) was recovered by addition of 3.5 mL Methanol-MilliQ water 50% (v/v) pre-chilled at -40 °C and 120 μL of U-$^{13}C$- cell extract. 3.5 mL of chloroform 100% pre-chilled at -40 °C was added in order to extract intracellular metabolites as described by [27].

## Analytical methods

### *Micro-titer plate assays*

Ninety-six well plate assays were prepared by adding 100 μL of synthetic medium with 20 g/L glucose, Tween-80 (420 mg/L) and ergosterol (10 mg/L). The initial pH of the medium was adjusted using 2 M HCl and 2 M KOH. $(NH_4)_2SO_4$ was used as the nitrogen source and the $SO_4^{2-}$ concentration was kept constant at 38 mM by addition of $K_2SO_4$ to compensate for the decrease in $SO_4^{2-}$ from $(NH_4)_2SO_4$. Cells were inoculated

in each well to a starting $OD_{660}$ of 0.1. Plates were covered with Nunc™ sealing tape (Thermo Scientific) and incubated at 30 °C with constant shaking at 200 rpm. OD660 was measured regularly in a GENios pro plate reader (Tecan Benelux, Giessen, The Netherlands).

### Metabolite quantification

Quantification of intracellular trehalose, glycolytic, TCA cycle and PPP intermediates was performed as described by [28]; amino acids were quantified according to [29], nucleotides as described in [30] and coenzymes were measured using LC-MS/MS as reported by [31]. Intra- and extracellular ammonium was quantified using ultra-high performance liquid chromatography with isotope dilution mass spectrometry (UHPLC-IDMS) as described by [25]. Quantification of extracellular metabolites was performed using HPLC as described in [32]. Cellular concentrations were estimated using the metabolite content per $g_{CDW}$ (μmol/$g_{CDW}$) and the average cell volume including dry matter ($mL_{WC}/g_{CDW}$), which was determined using a Z2 Coulter counter (50 μm aperture, Beckman, Fullerton, CA) [33].

### Proteomic analysis

U-$^{13}$C-labelled *S. cerevisiae* biomass was prepared as described by [34] and used as internal standard for relative protein quantification. Cell suspensions of the sample biomass and internal standard were mixed 1:1 based on the $OD_{600}$, washed with milli-Q and freeze-dried. Proteins were extracted by grinding the freeze-dried biomass with pestle and mortar, which were precooled with liquid nitrogen. After grinding, 2 mL of 50 mM phosphate buffer (PBS) with 200 mM NaOH was added to extract proteins. The soluble protein fraction was separated from the cell debris by centrifugation at 13,300 rpm for 15 min. Proteins were precipitated overnight in cold acetone at -20 °C by adding 4 parts of cold acetone to 1 part of protein solution. After washing and drying the protein pellet was dissolved in 400 μL of 100 mM ammonium bicarbonate (ABC) with 6 M urea. Of this solution, 20 μL was further processed; proteins were reduced by addition of tris(2-carboxyethil)phosphine (TCEP) to a final concentration of 10 mM and incubating for 60 min at room temperature. Proteins were alkylated by addition of Iodoacetamide (IAM) to a final concentration of 10 mM and incubating for 60 min at room temperature. Prior to digestion the protein solution was 6 times diluted by addition of 100 μL of 100 mM ABC to dilute the urea concentration to 1 M. Proteins were digested by addition of trypsin (trypsin singles, proteomics grade, Sigma-Aldrich) in a 1:100 ratio and incubating at 37 °C for 16 h. The digested protein mixture was purified and concentrated using an in-house made SPE pipette tip using 5 μm particles of Reprosil-Pur $C_{18}$-Aq reversed phase material (Dr. Maisch GmbH, Ammerbuch-Entringen, Germany).

Digested peptides were separated using nanoflow chromatography performed using a vented column system essentially as described by [35] and a 2-dimensional precolumn (RP-SCX-RP). Analytical columns of 50 μm id were prepared with a 1 mm Kasil frit and packed with 5 μm particles of Reprosil-Pur $C_{18}$-Aq reversed phase material to a length of 40 cm. The capillary RP-SCX-RP precolumn of 150 μm id was prepared with a 1 mm Kasil frit and packed with 5 μm particles of Reprosil-Pur C18-Aq reversed phase material to a length of 17 mm, 5 μm particles of PolySulfoethyl a strong cation exchange material for 60 mm and again 5 μm particles of Reprosil-Pur $C_{18}$-Aq reversed phase material for 17 mm (total length 94 mm). The different column materials were kept separated from each other by insertion of a piece of glass wool. The used LC equipment and solvents were similar to [36]. Each sample analysis consisted of six fractionations. In the first fraction the peptides are injected and trapped on the precolumn by applying 100% solvent A for 10 min. Then a first linear gradient was applied from 4 to 35% B in 75 min. After this, a linear gradient to 80% B was followed for 6 min and then 3 min of 80% B. Finally the column was reconditioned for 26 min with 100% A. In the following 5 fractionations, peptides were eluted by 10 μL injections of respectively 5, 10, 50, 250 or 1000 mM ammonium formate pH 2.6 from the autosampler (followed by 100% A for 10 min). Again a first linear gradient was applied from 4 to 35% B in 75 min, followed by a second linear gradient to 80% B for 6 min and then 3 min of 80% B. After each fraction the column was reconditioned for 26 min with 100% A. This results in six fractionations per sample with a total run-time of 12 h per sample. For each analysis ~10 μg of protein was injected.

Mass spectrometry was performed using a protocol derived from [36] and similar to [37]. Briefly explained, full scan MS spectra (from m/z 400–1500, charge states 2 and higher) were acquired at a resolution of 30,000 at m/z 400 after accumulation to a target value of $10^6$ ions (automatic gain control). Nine data-dependent MS/MS scans (HCD spectra, resolution 7,500 at m/z 400) were acquired using the 9 most intense ions with a charge state of 2+ or higher and an ion count of 10,000 or higher. The maximum injection time was set to 500 ms for the MS scans and 200 ms for the MS/MS scan (accumulation for MS/MS was set to target value of $5 \times 10^4$). Dynamic exclusion was applied using a maximum exclusion list of 50, one repeat count, repeat duration of 10 s and exclusion duration of 45 s. The exclusion window was set from −10 to + 10 ppm relative to the selected precursor mass.

Data processing and analysis was performed similarly to [36]. Briefly, MS/MS spectra were converted to

Mascot Generic Files (MGF) using Proteome Discoverer 1.4 (ThermoFisher Scientific) and DTASuperCharge version 2.0b1 [38]. MGF's from the 6 SCX fractions of the same sample were combined using MGFcombiner version 1.10 [38]. The samples were analyzed with Mascot v2.2.02 search engine (Matrix Science, Boston, MA, USA). As reference proteome the Uniprot [39] proteome of *Saccharomyces cerevisiae* strain ATCC 204508/288c (ID: UP000002311; 6634 sequences) was used.

Carbamidomethyl cysteine was set as a fixed modification and oxidized methionine as a variable modification. Trypsin was specified as the proteolytic enzyme, and up to three missed cleavages were accepted. Mass tolerance for fragment ions was set at 0.05 Da and for precursor peptide ions at 10 ppm. Peptides with Mascot score <10 were removed and only the highest scoring peptide matches for each query listed under the highest scoring protein (bold red) were selected. Proteins were quantified using MSQuant version 2.0b7 [38] by importing the Mascot results html file with the corresponding raw mass spectrometric data files. MSQuant automatically calculated peptide and protein ratios by using a $^{13}C$ quantitation method (in quantitationmodes.xml), containing 7 modifications based on the amount of carbon atoms each amino acid contains. The difference in mass between $^{12}C$ and $^{13}C$ is 1.00335 Da. Resulting in mass shifts of 2 (glycine), 3 (ASC), 4 (NDT), 5 (EQMPV), 6 (RHILK), 9 (FY) or 11 (W) carbon atoms. Quantification was restricted to peptides with Mascot score ≥25, it is considered that a protein is up regulated when the concentration of protein is at least 50% higher in one strain compared to the other, growing at the same environmental condition. On the other hand, proteins identified with 2 or more confidence peptides with Mascot score ≥25 in one strain but not in the other are considered "unique proteins".

## Results

### Effect of extracellular $NH_3$ concentration on growth rate

To identify whether the elimination of the ammonium permeases will eliminate $NH_4^+$ uptake and result in $NH_3$ diffusion as the sole mechanism, all permeases (Mep1, Mep2, and Mep3) were knocked-out. This resulted in strain IMZ351 (Additional file 1). Relative specific aerobic growth rates in micro-titer plate ($\mu_{MTP}$) of IMZ351 (*Δmep*) and the control strain IME169 (Mep1, Mep2, Mep3) were compared at varying initial pH values and $(NH_4)_2SO_4$ concentrations under aerobic conditions (Fig. 1). The concentration of $NH_3$ at a given $(NH_4)_2SO_4$ concentration is dependent on the extracellular pH. Note that increasing the pH significantly increases the $NH_3$ concentration. However, because the $pKa = 9.25$ strongly favors the charged form, the $NH_4^+$ concentration remains relatively unchanged, at between pH 3 and 7.

The growth rate of IME169 reached a maximum at approximately 20 mM $NH_X$. The growth rate was negatively affected by increasing pH values (Fig. 1a), an expected effect caused by the deviation from the optimum pH =5. On the other hand, it was observed that the strain IMZ351 increased its growth rate with increasing pH values (Fig. 1b). Consequently, plotting the specific growth rate as a function of the $NH_3$ concentration revealed a clear correlation between the two variables (Fig. 1c), indicating that the growth of IMZ351 was dependent on $NH_3$ concentration whereas IME169 growth was dependent on $NH_4^+$ concentrations. This supports the hypothesis that deletion of Mep proteins leads to a change in the main uptake mechanism, from $NH_4^+$ uniport to $NH_3$ diffusion. Clearly, diffusion is also present in the wild type. But, because of the electrochemical-based driving force, the concentration gradient for diffusion is actually in the direction of export rather than import. Thus, $NH_X$ uptake can only take place in the Mep-dependent transport mechanism.

If the Δ*mep* strain (IMZ351) indeed relied on diffusion of $NH_3$ to supply nitrogen to the cell, then the specific rate of N-uptake ($-q_N$, in mol N/$g_{CDW}$/h) is dependent on the $NH_3$ concentration gradient between extracellular space and cytosol ($[NH_3]_{EC}$-$[NH_3]_{cyt}$, in mmol/L). The rate of $NH_3$ uptake can be described by the apparent permeability coefficient ($P_{1a}$, in m/h) of the membrane, the biomass specific mass transfer area ($a_m$, in this study 3.22 $m^2/g_{CDW}$), and the concentration gradient: $-q_N = P_{1a}\ a_m([NH_3]_{EC} - [NH_3]_{cyt})$. Under nitrogen-limited conditions, the growth rate will be dependent on the extracellular $NH_3$ concentration, i.e., $\mu = \chi_N^{-1} - q_N$, with $\chi_N$ representing the biomass N-content (usually 0.148 mol N/C-mol biomass or $5.60 \times 10^{-3}$ mol N/$g_{CDW}$ [40]).

Based on this dependency, the $NH_3$ permeability coefficient for batch conditions can be estimated. Assuming that the $NH_3$ extracellular concentration is much higher than the cytosolic concentration, the previous dependency can be approximated by $-q_N = P_{1a}\ a_m[NH_3]_{EC}$. With the array of measured $\mu_{MTP}$ as a function of the initial $NH_3$ concentration (Fig. 1c), the $NH_3$ permeability coefficient is estimated as $P_{1a} = 0.01$ m/h. This value is two orders of magnitude below values reported in literature. This large deviation from the permeability measured in vitro could be due to different membrane compositions, but above all it is the assumption of negligible intracellular $NH_X$ concentration, which has an impact on the value obtained. The estimated value therefore represents the lower limit of permeability rather than a precise measure.

### Intracellular and extracellular $NH_X$ ratios under N-limiting conditions

The micro-titer assay described above showed a clear link between the extracellular $NH_3$ concentration and

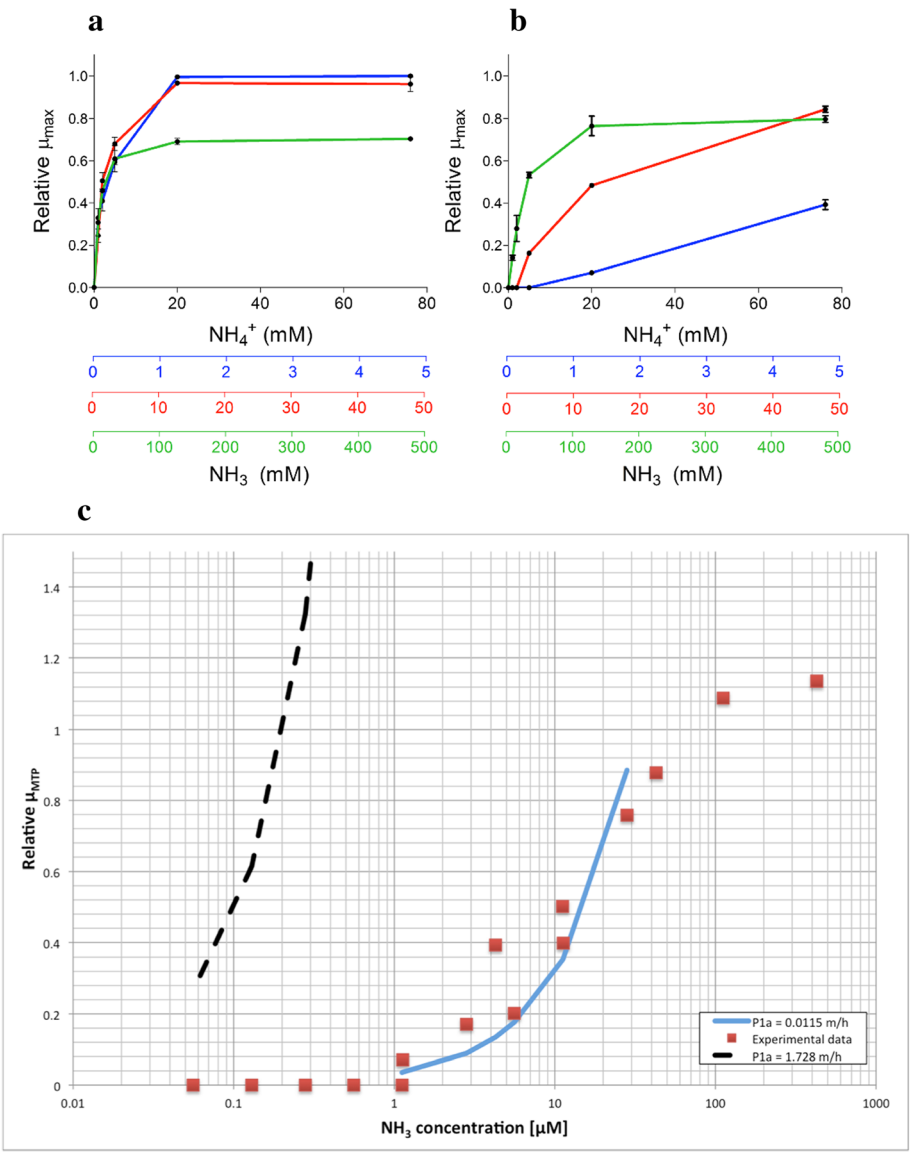


**Fig. 1** Relative specific growth rate in micro-titer plate ($\mu_{MTP}$) of (**a**) IME169 (reference strain) and (**b**) IMZ351 (Δ*mep*) at different pH and extracellular $NH_X$-concentrations, pH = 5 (*blue*), pH = 6 (*red*) and pH = 7 (*green*) in synthetic medium with glucose supplemented with Tween-80 (420 mg/L) and ergosterol (10 mg/L). **c** Relative specific growth rates in micro-titer plate ($\mu_{MTP}$) of IMZ351 at different $NH_3$-concentrations irrespective of extracellular pH. Growth rates were determined from exponentially growing cells cultured in 100 μL synthetic medium in 96 well plates with $OD_{660}$ measurements taken every 15 min. The $SO_4$ concentration was kept constant at 38 mM by supplementation with $K_2SO_4$. Data are presented as averages and standard deviations of duplicate experiments, relative to the average growth rate of IME169 at pH = 5, with 76 mM $NH_4^+$ ($\mu_{max} = 0.21\ h^{-1}$). The continuous blue line represents an apparent permeability coefficient of 0.0115 m/h (0.32 $10^{-3}$ cm/s), calculated using least squares in the linear region of the experimental data ($R^2 = 0.73$); the discontinuous black line shows the trend of the growth rate if an apparent permeability coefficient of 1.728 m/h (48 $10^{-3}$ cm/s) is assumed [17]

the growth rate of IMZ351, but these results cannot provide insights into the intracellular metabolism. Moreover, the absence of pH control and monitoring of dissolved oxygen concentration could potentially bias these results. In order to perform a detailed analysis of the resulting strain physiology in response to different mechanisms of $NH_X$ assimilation, aerobic N-limited chemostat cultures were carried out at varying pH values (pH = 5, pH = 6, pH = 7). Extracellular and intracellular metabolite measurements were performed at each steady-state condition. The aerobic N-limited conditions were selected to observe the energetic effect of $NH_3$-diffusion based on differences in specific oxygen consumption rates ($-q_{O2}$) between strains. Additionally, the use of N-limited conditions reduced the residual $NH_X$ and so increased the accuracy of the intracellular $NH_X$ measurements.

To ensure that the differential effect of pH and $NH_X$ concentration between the two strains were indeed based on differences in transport mechanisms, the cytosolic/extracellular $NH_X$ ratio was determined for both strains. If $NH_4^+$ were the only species being transported into the cell, then the uptake rate and the cytosolic/extracellular $NH_X$ ratio at steady state under N-limiting conditions would depend on the membrane potential. By contrast, if $NH_3$ were the only species being transported into the cell, then the $NH_X$-uptake rate and cytosolic/extracellular $NH_X$ ratio would depend only on the $NH_3$ concentration gradient across the cell membrane (Additional file 1). In other words, the two transport mechanisms can be discriminated on the basis of their different cytosolic/extracellular $NH_X$ ratios (Table 2). Furthermore, because the growth rate is similar for all cultivations and $NH_X$ is the limiting substrate, the cytosolic concentration of this compound was expected to be similar (if not the same), regardless of the transport mechanism, to support the same downstream nitrogen fluxes.

However, the cytosolic $NH_X$ concentration cannot be measured directly. Current metabolomic approaches allow only for whole-cell quantifications, which from now on will be called intracellular (IC) measurement. In the case of $NH_X$, previous works [41, 42] suggest significant accumulation and storage of $NH_X$ in the vacuole, which means that the whole-cell measurement and the cytosolic concentration could differ significantly. To account for vacuolar storage, the measured $NH_X$ ratios were compared with expected maximum and minimum ratios (IC/EC) based on assumptions for vacuolar diffusion (Additional file 1). Interestingly, the expected difference in ratios still allows for a clear separation of mechanisms in the presence of vacuolar storage.

In line with our hypothesis, the experimental data showed ratios with a difference of at least one order of magnitude between IME169 (Mep1, Mep2, Mep3) and IMZ351 (*Δmep*) (Table 2). For IMZ351, the IC/EC ratios measured experimentally corresponded well with the predicted ratios. However, while the IC/EC ratio for IME169 was predicted to increase with extracellular pH, it actually varied between 210 and 300 under the experimental conditions (Table 2) - which might indicate that, under these conditions, the ratio is determined by the affinity of the ammonium permeases and not by the thermodynamic driving force. Besides differences in IC/EC ratios, a substantially higher intracellular $NH_X$ concentration was observed for IMZ351.

### Estimation of the $NH_3$ permeability coefficient at steady state under N-limiting conditions

Under N-limiting conditions, it can be assumed that transport of the N-source is the limiting factor for growth in both strains. In IMZ351, the diffusion rate is determined, as explained earlier, by the $NH_3$ permeability and the concentration gradient across the plasma membrane (($[NH_3]_{EC}$-$[NH_3]_{cyt}$). While the concentration in the extracellular space ($[NH_3]_{EC}$) is measured directly, the cytosolic concentration ($[NH_3]_{cyt}$) needs to be estimated from the whole-cell measurement (IC), the specific nitrogen uptake rate ($-q_N$), and assumptions regarding the intracellular $NH_X$ distribution (Additional file 1). Here, it is assumed that the cytosol volume represents 70% of the cell volume, the vacuolar volume is 14% and the mitochondrial volume is about 1% of the total cell volume [43].

Additionally, $NH_3$ transport processes between different compartments are assumed to operate close to thermodynamic equilibrium -and since no transport proteins that could translocate $NH_X$ between compartments are described in literature, passive diffusion of $NH_3$ between

**Table 2** Intracellular and extracellular $NH_X$ concentrations of IME169 (reference strain) and IMZ351 (**Δ***mep*) measured at steady state at varying pH values from aerobic N-limited chemostats in synthetic medium with glucose at a dilution rate of 0.05 $h^{-1}$ and the corresponding $NH_X$ IC/EC ratios. For calculation of predicted intracellular/extracellular ratios with compartmentalization three compartments were considered: cytosol, mitochondria and vacuole. The ratios were calculated as the maxima and minima of a sensitivity analysis where the following critical variables were considered: vacuolar volumes (between 25 and 14% intracellular volume), cytosolic pH (between 6 and 7) and vacuolar pH (between 4 and 5.5). The data represent average and mean deviation of triplicates

| Strain | pH | Average cell volume ($mL_{IC}/g_{CDW}$) | Biomass concentration ($g_{CDW}/L_{broth}$) | Intracellular $NH_X$ ($mmol/L_{IC}$) | Extracellular $NH_X$ ($mmol/L_{EC}$) | Measured IC/EC ratio | Predicted IC/EC equilibrium ratio range | |
|---|---|---|---|---|---|---|---|---|
| | | | | | | | Maximum | Minimum |
| IME169 Uniport $NH_4^+$ | 5.0 | 2.59 ± 0.04 | 7.00 ± 0.02 | 1.74 ± 0.14 | 0.008 ± 0.001 | 219 ± 39 | $5.44 \times 10^3$ | 108 |
| | 6.0 | 2.43 ± 0.04 | 7.45 ± 0.01 | 3.16 ± 0.16 | 0.011 0.003 | 302 ± 40 | $5.44 \times 10^4$ | $1.09 \times 10^3$ |
| | 7.0 | 2.62 ± 0.02 | 7.73 ± 0.03 | 3.33 ± 0.09 | 0.013 ± 0.001 | 254 ± 10 | $5.44 \times 10^5$ | $1.09 \times 10^4$ |
| IMZ351 Diffusion $NH_3$ | 5.0 | 2.01 ± 0.08 | 6.44 ± 0.01 | 10.5 ± 0.7 | 6.99 ± 0.28 | 1.5 ± 0.1 | 2.57 | 0.05 |
| | 6.0 | 2.00 ± 0.04 | 7.37 ± 0.04 | 10.9 ± 0.6 | 2.61 ± 0.09 | 4.2 ± 0.3 | 25.7 | 0.5 |
| | 7.0 | 2.31 ± 0.09 | 7.73 ± 0.01 | 7.48 ± 0.7 | 0.57 ± 0.02 | 13.2 ± 1.3 | 255 | 5 |

vacuole and cytosol, as well as between cytosol and mitochondria, are assumed.

With these assumptions and measurements, a linear equation system is set up to calculate the missing variables (Additional file 1). The apparent permeability coefficient varies between 0.03 m/h and 2.73 m/h (Table 3), decreasing with pH, as has also been observed for other biological systems [44]. It should also be mentioned that, for an extracellular pH of 5, the assumptions for vacuolar size and pH have to be adjusted to 25% of the cell volume and 4.2, respectively, in order to obtain a positive $NH_3$ concentration gradient between extracellular space and cytosol.

## Impact of $NH_3$-diffusion on the physiology and metabolic fluxes of *S. cerevisiae* under aerobic N-limiting conditions

### *Effect of diffusion on the specific consumption and production rates*

The effect of $NH_3$-dependent mechanism of nitrogen uptake on ATP consumption was determined based on a simple metabolic model. All relevant q-rates and physiological parameters are shown in Table 4. The ATP production rate was calculated based on the oxygen consumption rate (1.9 mol ATP/mol $O_2$) and the rate of alcoholic fermentation (1 mol ATP/mol ethanol) under respirofermentative conditions, which was observed under N-limiting conditions [45]. Contrary to the expectation of a reduced ATP cost per assimilated N-mole, IMZ351 consumed more ATP per mole of N-assimilated than IME169. So secondary effects like increased N-starvation stress could lead to higher ATP consumption. This hypothesis is further supported by an observed decrease in N-conent and higher C/N consumption, together with a higher production of reserve carbohydrates (i.e., trehalose and glycogen), which are related to stress response.

### *Intracellular metabolite concentrations*

IMZ351 showed decreased biomass N-content when compared to IME169, suggesting that deletion of Mep genes resulted in an altered cellular response in nitrogen-limited chemostat cultures. To investigate physiological effects caused by the decreased specific $NH_X$ uptake rates, the concentrations of intracellular metabolites involved in carbon and nitrogen metabolism were measured (Additional file 1). While, surprisingly, the intracellular $NH_X$ concentration was actually significantly higher in IMZ351, the intracellular concentration of the product of the most prominent entry route for $NH_X$ assimilation, L-glutamate (Glu), was comparable in both strains at each pH. The L-glutamine concentration, which is the end product of the alternative route of $NH_X$ assimilation via the GS-GOGAT system, was lower for IMZ351 compared to the reference strain, but increased with pH. Downstream, the concentration of amino acids synthesized in the mitochondria -L-alanine, L-valine and L-lysine- were significantly lower in IMZ351. Furthermore, the intracellular trehalose concentration -which is an indicator of cellular stress and/or nitrogen limitation [46]- was significantly higher in IMZ351 at all pH conditions.

### *Effects of $NH_3$ diffusion on the protein levels*

Alteration of the $NH_X$ transport mechanism resulted in changes in cellular metabolism, which were also related to changes in the protein levels [47, 48]. The measurement of relative protein levels showed changes in more than 300 different proteins, but in amounts that varied between strains in the different pH conditions. The concentration of certain proteins were low and could only be observed in one of the strains. Those proteins are called from "unique proteins", although in this case the word "unique" does not imply that they are totally absent from the other strains/conditions, but only that their levels are in some cases below the detection tershold. While our analytical method cannot provide an answer on whether proteins are present or absent in the protein levels, then, these 'unique' proteins can be considered a especial subset of up/down regulated proteins. Nineteen proteins were consistently found as unique in IMZ351, but not in the reference strain (IME169) at all pH conditions; i.e., they were expressed at measurable levels in IMZ351 while not in IME169 (Additional file 1). Of these, of particular interest were Rav1 (regulator of the activity of vacuolar ATPase acitivty), Hog1 (global regulator of stress responses), and Mck1 (threonine/serine protein kinase that regulates DNA replication [49], C-metabolism, and protein kinase A activity [50]).

GO-term cluster analysis revealed that among the proteins with at least 50% increased levels in IMZ351 were related to stress-response terms, i.e., DNA replication stress and inefficient DNA replication [51], as well as autophagy and decreased protein production [52]. In that

**Table 3** Estimation of the apparent permeability coefficient of ammonium for IMZ351 (Δ*mep*) into the plasma membrane

| Strain | $pH_{EC}$ | $pH_{vac}$ | Cytosolic $NH_3$ (μmol/$L_{Cyt}$) | Extracellular $NH_3$ (μmol/$L_{EC}$) | Estimated Cyt/EC ratio | Apparent permeability coefficient (m/h) |
|---|---|---|---|---|---|---|
| IMZ351 | 5.0[a] | 4.2[a] | 0.37 | 0.39 | 0.030 | 2.73[a] |
| | 6.0 | 4.5 | 1.31 | 1.47 | 0.283 | 0.37 |
| | 7.0 | 4.5 | 0.90 | 3.16 | 0.902 | 0.03 |

[a] In this particular case, a numerical solution to the system of algebraic equations that estimates $P_{1a}$ (Additional file 1) is achieved only if the vacuolar pH was 4.2 and the vacuolar volume considered was 25% of the total cell volume

**Table 4** Overview of measured extracellular fluxes and N-content of IME169 (reference strain) and IMZ351 (**Δ***mep*) during N-limited aerobic chemostats in synthetic medium with glucose at a dilution rate of 0.05 $h^{-1}$ at different extracellular pH

| Strain | $pH_{EC}$ | μ | $-q_S$ | $-q_{O2}$ | $q_{CO2}$ | $q_{Ethanol}$ | $-q_N$ | N-content | $Y_{XS}$ | C/N consumption | $q_{ATP}$ | $q_{ATP}/-q_N$ |
|---|---|---|---|---|---|---|---|---|---|---|---|---|
| | | 1/h | $mmol/g_{CDW}/h$ | $mmol/g_{CDW}/h$ | $mmol/g_{CDW}/h$ | $mmol/g_{CDW}/h$ | $mmol/g_{CDW}/h$ | $mmol\ N/g_{CDW}$ | $g_{CDW}/g_{Glc}$ | C-mol/N-mol | $mmol/g_{CDW}/h$ | mol ATP/mol N |
| IME169 | 5.0 | 0.053 ± 0.001 | 3.862 ± 0.050 | 1.643 ± 0.006 | 7.028 ± 0.015 | 4.601 ± 0.223 | 0.251 ± 0.001 | 4.70 ± 0.01 | 0.077 ± 0.001 | 92.3 ± 1.3 | 7.72 ± 0.22 | 30.8 ± 0.9 |
| | 6.0 | 0.052 ± 0.001 | 3.398 ± 0.013 | 1.468 ± 0.004 | 6.157 ± 0.010 | 4.438 ± 0.055 | 0.223 ± 0.004 | 4.30 ± 0.08 | 0.085 ± 0.001 | 91.4 ± 1.7 | 7.23 ± 0.05 | 32.4 ± 0.6 |
| | 7.0 | 0.051 ± 0.001 | 2.953 ± 0.013 | 1.273 ± 0.007 | 5.218 ± 0.020 | 3.608 ± 0.038 | 0.208 ± 0.004 | 4.06 ± 0.08 | 0.096 ± 0.001 | 104.1 ± 2.3 | 6.03 ± 0.04 | 28.9 ± 0.6 |
| IMZ351 | 5.0 | 0.047 ± 0.001 | 3.485 ± 0.025 | 1.390 ± 0.005 | 6.620 ± 0.014 | 4.735 ± 0.039 | 0.190 ± 0.008 | 4.00 ± 0.17 | 0.081 ± 0.001 | 110.1 ± 4.7 | 7.38 ± 0.04 | 38.9 ± 1.6 |
| | 6.0 | 0.047 ± 0.001 | 3.074 ± 0.017 | 1.223 ± 0.006 | 5.825 ± 0.028 | 4.404 ± 0.046 | 0.183 ± 0.003 | 3.91 ± 0.06 | 0.085 ± 0.001 | 100.8 ± 1.7 | 6.73 ± 0.05 | 36.7 ± 0.6 |
| | 7.0 | 0.048 ± 0.001 | 2.826 ± 0.031 | 1.239 ± 0.004 | 5.081 ± 0.009 | 3.639 ± 0.053 | 0.187 ± 0.003 | 3.88 ± 0.06 | 0.095 ± 0.001 | 90.7 ± 1.8 | 5.99 ± 0.05 | 32.0 ± 0.5 |

group, Rtp6 and Cps1 were found at higher levels and described to correlate with severe N-limitation state. While a significant up-regulation of proteins involved in various stress responses was observed, no significant differences in proteins involved in nitrogen catabolite repression (NCR) and central nitrogen metabolism were observed.

## Discussion

Based on the experimental and modeling results, it was shown that $NH_3$ diffusion is the main $NH_X$ transport mechanism in Mep-deficient strain IMZ351. Alternative mechanisms, like transport through $K^+$-channels, can be excluded. In particular, the aerobic micro-titer experiments showed that the growth rate was dependent on extracellular $NH_3$ concentration rather than the electrochemical gradient. Furthermore, the cytosolic/extracellular ratio of $NH_X$ for IMZ351 under aerobic N-limiting conditions was consistent with the ratio predicted for $NH_3$ diffusion, but not with any transport mechanism dependent on the cell membrane potential or pmf.

By contrast with IMZ351, the observed IC/EC ratio for IME169 remained relatively constant and at least one order of magnitude higher than the ratios observed in IMZ351 across all pH values. Nevertheless, the experimental ratios did not match the predicted ratios at pH 6 and pH 7, which could be explained by a limitation in affinity ($K_M$) of the Mep proteins rather than the thermodynamic driving force. Notwithstanding this, our results for IME169 at different pH values clearly show that $NH_4^+$ is the transported species, opposing previous studies suggesting that Mep proteins and other Amt-class transporters carry uncharged $NH_3$ across the membrane [42, 53].

The metabolic profile in both strains presented clear differences, like a significantly higher concentration of intracellular $NH_X$ and trehalose in the strain IMZ351. While the cause of this remains unanswered, the observation raises questions about the signaling pathways for N-limitation. Our experimental results suggest that intracellular $NH_X$ is not involved in signaling.

Proteomic analysis revealed significantly higher levels of proteins related to recycling of N-compounds (proteins, amino acids) and general cellular stress responses, suggesting an altered cellular response to N-limitation. However, in view of the higher intracellular $NH_X$ concentration (Table 2) and the generally comparable concentrations of most intracellular N-based metabolites (Additional file 1), this appears to be unrelated to any particular signaling metabolite in the intracellular space. Mep1 and Mep2 have been described as $NH_4^+$ transceptors, not only responsible for transport across the cell membrane but also acting as cAMP-independent activators of the protein kinase A (PKA) signaling cascade; this signal is triggered due to conformational changes in Mep1 and Mep2 after binding with ammonium [54]. In the absence of extracellular $NH_4^+$, no ammonium permease-mediated signal is sent to the PKA complex, leading to its inactivation and subsequent repression of glycolytic genes and of genes involved in cellular growth and proliferation, and in particular to an up-regulation of genes responsible for the cellular stress response mediated by STRE (stress response element) [55]. This hypothesis is supported indirectly by the presence of

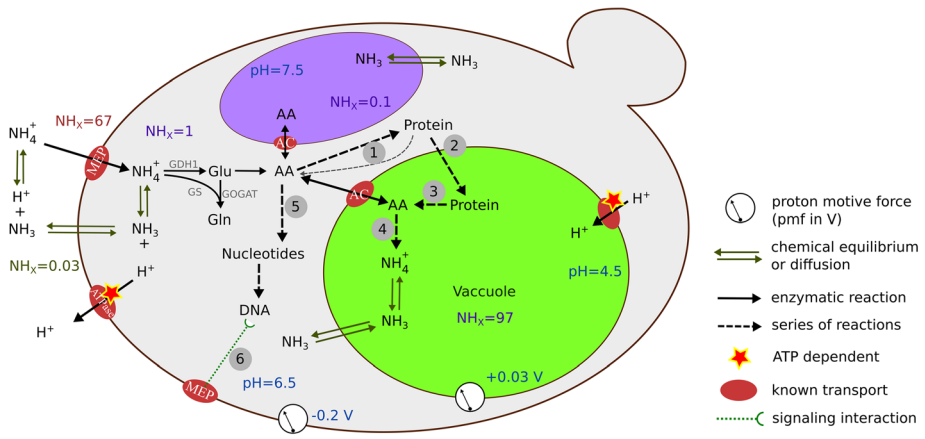


**Fig. 2** Summary of mechanisms and hypotheses for IME169 (reference strain) and IMZ351 (Δmep). For both strains, the main reactions of nitrogen incooperation are GS-GOGAT, Gdh1, Gdh2 and Gdh3, fueling amino acids and biomass synthesis, esp. protein (1) and nucleotides (5). The NH4 transporter proteins Mep1 and Mep2 work as transceptors (6), signaling the presence of ammonium and activate a yet unidentified signaling cascade [57], possibly protein kinase A (PKA) as described in previous works [54, 57]. In the absence of MEP-proteins there is a constitutive down-regulation/repression of PKA and up-regulation/activation of genes associated with autophagy and DNA replication stress (see main text). These stress responses lead to decreased DNA replication and protein biosynthesis and increased protein turnover (3). The protein turnover could result in production of amino acids and/or higher NHX concentrations (4), amino acid recycling and trehalose overproduction

Mck1, which was one of the proteins only found in IMZ351 but not in the reference strain.Mck1 is a known transcriptional regulator, PKA inhibitor, and modulator of other cellular processes, such as DNA replication and protein degradation. We thus speculate that a constitutive up-regulation of the cellular stress response is generated upon deletion of the genes encoding the ammonium permeases. Proteins involved in various stress responses, in particular DNA replication stress, decreasing protein synthesis, increasing protein turnover, and increased cell-wall protective agents (trehalose, cell wall repair systems) [56] are expressed in IMZ351 (Fig. 2). However, whether this fully explains the metabolite profile of IMZ351 and especially the increase in intracellular $NH_X$ and the decrease in mitochondrial amino acids, or whether additional responses are also involved is yet to be ascertained.

This (stressed) phenotype of IMZ351 revealed the system's nature –while the cost for the transport could be reduced, secondary responses lead to ATP consumption and the aim of improved energy efficiency cannot be achieved without additional steps. This increased energy consumption interferes with the ability to apply anaerobic production conditions without decreasing the negative physiological effects from deletion of Mep proteins.

## Conclusions

The underlying goal of this study was to engineer membrane potential-decoupled $NH_X$ assimilation for use in bulk N-containing chemical production. Although diffusion of $NH_3$ metabolically conserves ATP in the N-assimilation process, the observed metabolic rates did not show this energy conservation improvement. The different degrees of N-limitation in both strains led to an uncoupling between of metabolic ATP saving from biomass production, as observed from the experimental N-biomass content, trehalose concentration and $q_{ATP}/q_N$ ratio.

To enable future industrial (anaerobic) applications, elucidation and subsequent engineering of this stress response will be required.

## Additional file

**Additional file 1:** Contains details on strain construction and confirmation, additional details on calculations and additional metabolome and proteome measurements. (PDF 1095 kb)

### Abbreviations

$NH_3$: Ammonia; $NH_4^+$: Ammonium; $NH_X$: Sum of $NH_3 + NH_4^+$ (total ammonium); $P_{1a}$: Permeability coefficient; PKA: Protein kinase A; pmf: Proton motive force; STRE: Stress response element; UHPLC-IDMS: Ultra-high performance liquid chromatography with isotope dilution mass spectrometry

### Acknowledgments

The authors wish to thank Martijn Pinkse, Sebastiaan de Bruin, Erik de Hulster, Reza Maleki Seifar, Angela ten Pierick, Marijke Luttik, Tim Vos and Pascale Daran-Lapujade for their valuable contribution to this work. Special thanks to Prof. Dr. Ir. Sef Heijnen and Prof. Dr. Jack Pronk for their valuable feedback and critical revision of this manuscript. The authors especially thank colleagues helping with rapid sampling experiments: Camilo Suárez-Méndez, Cristina Bernal, Angel Sevilla, Francisca Lameiras, Leonor Guedes da Silva, Mariana Velasco-Alvarez and Mihir Shah.

### Funding

This work was performed within the BE-Basic R&D program (http://www.be-basic.org), which was granted a FES subsidy from the Dutch Ministry of Economic Affairs, Agriculture and Innovation (EL&I). The author HFCR received a scholarship from CONACyT (Scholarship number: 212059).

### Availability of data and materials

The datasets supporting the conclusions of this article are included within the article and attached supplementary materials.

### Authors' contributions

HFCR: drafted and edited the manuscript, performed chemostat experiments, metabolomics analysis, data collection and analysis. NM performed strain constructions and micro-titer plate experiments, wrote the respective manuscript section and reviewed the manuscript. WH performed proteomics measurements and data analysis, and contributed to the respective manuscript section. MP supervised the proteomics measurements and contributed to the interpretation of measurement data. AJAM contributed to the design of the experiments and reviewed the manuscript. JMD contributed to the design of the experiments and reviewed the manuscript. SAW contributed to the design of the experiments and reviewed the manuscript. All authors contributed equally reviewing this manuscript. All authors read and approved the final manuscript.

### Competing interests

The funders had no role in study design, data collection and interpretation, or the decision to submit the work for publication. The authors declare that they have no competing interests.

### Consent for publication

Not applicable.

### Ethics approval and consent to participate

Not applicable. This article does not contain any studies with human participants or animals performed by any of the authors.

### Author details

[1]Department of Biotechnology, Delft University of Technology, van der Maasweg 9, 2629HZ Delft, The Netherlands. [2]Present Address: Evolva Biotech A/S, Lersø Parkallé 42, 2100 København Ø, Denmark. [3]Present Address: Nederlands Forensisch Instituut (NFI), Laan van Ypenburg 6, 2497 GB Den Haag, The Netherlands. [4]Division of Industrial Biotechnology, School of Biotechnology, KTH Royal Institute of Technology, AlbaNova University Center, SE 106 91 Stockholm, Sweden.

Received: 19 May 2016 Accepted: 20 December 2016
Published online: 17 April 2017

### References

1. Choi S, Song CW, Shin JH, Lee SY. Biorefineries for the production of top building block chemicals and their derivatives. Metab Eng. 2015;28:223–39.
2. Nielsen J, Larsson C, van Maris A, Pronk J. Metabolic engineering of yeast for production of fuels and chemicals. Curr Opin Biotechnol. 2013;24(3):398–404.
3. Hong KK, Nielsen J. Metabolic engineering of *Saccharomyces cerevisiae*: a key cell factory platform for future biorefineries. Cell Mol Life Sci. 2012; 69(16):2671–90.
4. Oldiges M, Eikmanns BJ, Blombach B. Application of metabolic engineering for the biotechnological production of L-valine. Appl Microbiol Biotechnol. 2014;98(13):5859–70.
5. Qian ZG, Xia XX, Lee SY. Metabolic engineering of *Escherichia coli* for the production of cadaverine: a five carbon diamine. Biotechnol Bioeng. 2011; 108(1):93–103.
6. Turk SC, Kloosterman WP, Ninaber DK, Kolen KP, Knutova J, Suir E, Schurmann M, Raemakers-Franken PC, Muller M, de Wildeman SM et al.

Metabolic engineering toward sustainable production of nylon-6. ACS Synth Biol. 2015;5:65–73.
7. van Maris AJ, Winkler AA, Kuyper M, de Laat WT, van Dijken JP, Pronk JT. Development of efficient xylose fermentation in *Saccharomyces cerevisiae*: xylose isomerase as a key component. Adv Biochem Eng Biotechnol. 2007; 108:179–204.
8. de Kok S, Kozak BU, Pronk JT, van Maris AJ. Energy coupling in *Saccharomyces cerevisiae*: selected opportunities for metabolic engineering. FEMS Yeast Res. 2012;12(4):387–97.
9. Weusthuis RA, Lamot I, van der Oost J, Sanders JP. Microbial production of bulk chemicals: development of anaerobic processes. Trends Biotechnol. 2011;29(4):153–8.
10. Milne N, Luttik MA, Cueto Rojas HF, Wahl A, van Maris AJ, Pronk JT, Daran JM. Functional expression of a heterologous nickel-dependent, ATP-independent urease in *Saccharomyces cerevisiae*. Metab Eng. 2015;30:130–40.
11. Franden MA, Pilath HM, Mohagheghi A, Pienkos PT, Zhang M. Inhibition of growth of *Zymomonas mobilis* by model compounds found in lignocellulosic hydrolysates. Biotechnol Biofuels. 2013;6(1):99.
12. Kumar P, Barrett DM, Delwiche MJ, Stroeve P. Methods for pretreatment of lignocellulosic biomass for efficient hydrolysis and biofuel production. Ind Eng Chem Res. 2009;48(8):3713–29.
13. Ullmann RT, Andrade SL, Ullmann GM. Thermodynamics of transport through the ammonium transporter *Amt-1* investigated with free energy calculations. J Phys Chem B. 2012;116(32):9690–703.
14. Magasanik B. Ammonia assimilation by *Saccharomyces cerevisiae*. Eukaryot Cell. 2003;2(5):827–9.
15. Marini AM, Soussi-Boudekou S, Vissers S, Andre B. A family of ammonium transporters in *Saccharomyces cerevisiae*. Mol Cell Biol. 1997;17(8):4282–93.
16. Hess DC, Lu W, Rabinowitz JD, Botstein D. Ammonium toxicity and potassium limitation in yeast. PLoS Biol. 2006;4(11):e351.
17. Antonenko YN, Pohl P, Denisov GA. Permeation of ammonia across bilayer lipid membranes studied by ammonium ion selective microelectrodes. Biophys J. 1997;72(5):2187–95.
18. Entian KD, Kotter P. Yeast genetic strain and plasmid collections. Yeast Gene Analysis, Second Edition. 2007; 36:629-666.
19. Nijkamp JF, van den Broek M, Datema E, de Kok S, Bosman L, Luttik MA, Daran-Lapujade P, Vongsangnak W, Nielsen J, Heijne WH, et al. De novo sequencing, assembly and analysis of the genome of the laboratory strain Saccharomyces cerevisiae CENPK113-7D, a model for modern industrial biotechnology. Microb Cell Fact. 2012;11:36.
20. Verduyn C, Postma E, Scheffers WA, Van Dijken JP. Effect of benzoic acid on metabolic fluxes in yeasts: a continuous-culture study on the regulation of respiration and alcoholic fermentation. Yeast. 1992;8(7):501–17.
21. Pronk JT. Auxotrophic yeast strains in fundamental and applied research. Appl Environ Microbiol. 2002;68(5):2095–100.
22. Verduyn C, Postma E, Scheffers WA, van Dijken JP. Physiology of *Saccharomyces cerevisiae* in anaerobic glucose-limited chemostat cultures. J Gen Microbiol. 1990;136(3):395–403.
23. Boer VM, Crutchfield CA, Bradley PH, Botstein D, Rabinowitz JD. Growth-limiting intracellular metabolites in yeast growing under diverse nutrient limitations. Mol Biol Cell. 2010;21(1):198–211.
24. Mashego MR, van Gulik WM, Vinke JL, Visser D, Heijnen JJ. *In vivo* kinetics with rapid perturbation experiments in *Saccharomyces cerevisiae* using a second-generation BioScope. Metab Eng. 2006;8(4):370–83.
25. Cueto-Rojas H, Maleki Seifar R, ten Pierick A, Heijnen S, Wahl A. Accurate measurement of the in vivo ammonium concentration in Saccharomyces cerevisiae. Metabolites. 2016;6(2):12.
26. Lange HC, Eman M, van Zuijlen G, Visser D, van Dam JC, Frank J, de Mattos MJ, Heijnen JJ. Improved rapid sampling for *in vivo* kinetics of intracellular metabolites in *Saccharomyces cerevisiae*. Biotechnol Bioeng. 2001;75(4):406–15.
27. Canelas AB, ten Pierick A, Ras C, Maleki Seifar R, van Dam JC, van Gulik WM, Heijnen JJ. Quantitative evaluation of intracellular metabolite extraction techniques for yeast metabolomics. Anal Chem. 2009;81(17):7379–89.
28. Niedenführ S, Pierick AT, van Dam PT, Suarez-Mendez CA, Nöh K, Wahl SA. Natural isotope correction of MS/MS measurements for metabolomics and C fluxomics. Biotechnol Bioeng. 2015;113(5):1137–1147.
29. de Jonge LP, Buijs NA, ten Pierick A, Deshmukh A, Zhao Z, Kiel JA, Heijnen JJ, van Gulik WM. Scale-down of penicillin production in *Penicillium chrysogenum*. Biotechnol J. 2011;6(8):944–58.
30. Maleki Seifar R, Ras C, van Dam JC, van Gulik WM, Heijnen JJ, van Winden WA. Simultaneous quantification of free nucleotides in complex biological samples using ion pair reversed phase liquid chromatography isotope dilution tandem mass spectrometry. Anal Biochem. 2009;388(2):213–9.
31. Maleki Seifar R, Ras C, Deshmukh AT, Bekers KM, Suarez-Mendez CA, da Cruz AL, van Gulik WM, Heijnen JJ. Quantitative analysis of intracellular coenzymes in *Saccharomyces cerevisiae* using ion pair reversed phase ultra high performance liquid chromatography tandem mass spectrometry. J Chromatogr A. 2013;1311:115–20.
32. Cruz AL, Verbon AJ, Geurink LJ, Verheijen PJ, Heijnen JJ, van Gulik WM. Use of sequential-batch fermentations to characterize the impact of mild hypothermic temperatures on the anaerobic stoichiometry and kinetics of *Saccharomyces cerevisiae*. Biotechnol Bioeng. 2012;109(7):1735–44.
33. Bisschops MM, Zwartjens P, Keuter SG, Pronk JT, Daran-Lapujade P. To divide or not to divide: a key role of *Rim15* in calorie-restricted yeast cultures. Biochim Biophys Acta. 2014;1843(5):1020–30.
34. Wu L, Mashego MR, van Dam JC, Proell AM, Vinke JL, Ras C, van Winden WA, van Gulik WM, Heijnen JJ. Quantitative analysis of the microbial metabolome by isotope dilution mass spectrometry using uniformly $^{13}C$-labeled cell extracts as internal standards. Anal Biochem. 2005;336(2):164–71.
35. Meiring HD, van der Heeft E, ten Hove GJ, de Jong APJM. Nanoscale LC-MS(n): technical design and applications to peptide and protein analysis. J Sep Sci. 2002;25(9):557–68.
36. Finoulst I, Vink P, Rovers E, Pieterse M, Pinkse M, Bos E, Verhaert P. Identification of low abundant secreted proteins and peptides from primary culture supernatants of human T-cells. J Proteomics. 2011;75(1):23–33.
37. Ebrahimi KH, Hagedoorn PL, Hagen WR. Self-assembly is prerequisite for catalysis of Fe(II) oxidation by catalytically active subunits of ferritin. J Biol Chem. 2015;290(44):26801–10.
38. Mortensen P, Gouw JW, Olsen JV, Ong SE, Rigbolt KT, Bunkenborg J, Cox J, Foster LJ, Heck AJ, Blagoev B, et al. MSQuant, an open source platform for mass spectrometry-based quantitative proteomics. J Proteome Res. 2010;9(1):393–403.
39. Uniprot C. UniProt: a hub for protein information. Nucleic Acids Res. 2015; 43(Database issue):D204–12.
40. Lange HC, Heijnen JJ. Statistical reconciliation of the elemental and molecular biomass composition of *Saccharomyces cerevisiae*. Biotechnol Bioeng. 2001;75(3):334–44.
41. Wood CC, Poree F, Dreyer I, Koehler GJ, Udvardi MK. Mechanisms of ammonium transport, accumulation, and retention in ooyctes and yeast cells expressing *Arabidopsis AtAMT1;1*. FEBS Lett. 2006;580(16):3931–6.
42. Soupene E, Ramirez RM, Kustu S. Evidence that fungal MEP proteins mediate diffusion of the uncharged species $NH_3$ across the cytoplasmic membrane. Mol Cell Biol. 2001;21(17):5733–41.
43. Uchida M, Sun Y, McDermott G, Knoechel C, Le Gros MA, Parkinson D, Drubin DG, Larabell CA. Quantitative analysis of yeast internal architecture using soft X-ray tomography. Yeast. 2011;28(3):227–36.
44. Ritchie RJ. The ammonia transport, retention and futile cycling problem in cyanobacteria. Microb Ecol. 2013;65(1):180–96.
45. Boer VM, de Winde JH, Pronk JT, Piper MD. The genome-wide transcriptional responses of *Saccharomyces cerevisiae* grown on glucose in aerobic chemostat cultures limited for carbon, nitrogen, phosphorus, or sulfur. J Biol Chem. 2003;278(5):3265–74.
46. Hazelwood LA, Walsh MC, Luttik MA, Daran-Lapujade P, Pronk JT, Daran JM. Identity of the growth-limiting nutrient strongly affects storage carbohydrate accumulation in anaerobic chemostat cultures of *Saccharomyces cerevisiae*. Appl Environ Microbiol. 2009;75(21):6876–85.
47. Kleijn R, Fendt SM, Schuetz R, Heinemann M, Zamboni N, Sauer U. Transcriptional control of metabolic fluxes and computational identification of the governing principles. FEBS J. 2010;277:27.
48. Kotte O, Zaugg JB, Heinemann M. Bacterial adaptation through distributed sensing of metabolic fluxes. Mol Syst Biol. 2010;6:355.
49. Ikui AE, Rossio V, Schroeder L, Yoshida S. A yeast GSK-3 kinase *Mck1* promotes *Cdc6* degradation to inhibit DNA re-replication. PLoS Genet. 2012;8(12):e1003099.
50. Quan Z, Cao L, Tang Y, Yan Y, Oliver SG, Zhang N. The yeast GSK-3 homologue *Mck1* is a key controller of quiescence entry and chronological lifespan. PLoS Genet. 2015;11(6):e1005282.
51. Burhans WC, Weinberger M. DNA damage and DNA replication stress in yeast models of aging. Subcell Biochem. 2012;57:187–206.
52. Onodera J, Ohsumi Y. Autophagy is required for maintenance of amino acid levels and protein synthesis under nitrogen starvation. J Biol Chem. 2005;280(36):31582–6.
53. Soupene E, Lee H, Kustu S. Ammonium/methylammonium transport (Amt) proteins facilitate diffusion of NH3 bidirectionally. Proc Natl Acad Sci U S A. 2002;99(6):3926–31.

54. Van Nuland A, Vandormael P, Donaton M, Alenquer M, Lourenco A, Quintino E, Versele M, Thevelein JM. Ammonium permease-based sensing mechanism for rapid ammonium activation of the protein kinase A pathway in yeast. Mol Microbiol. 2006;59(5):1485–505.
55. Thevelein JM, de Winde JH. Novel sensing mechanisms and targets for the cAMP-protein kinase A pathway in the yeast Saccharomyces cerevisiae. Mol Microbiol. 1999;33(5):904–18.
56. Martinez-Pastor MT, Marchler G, Schuller C, Marchler-Bauer A, Ruis H, Estruch F. The *Saccharomyces cerevisiae* zinc finger proteins *Msn2p* and *Msn4p* are required for transcriptional induction through the stress-response element (STRE). EMBO J. 1996;15(9):2227–35.
57. Conrad M, Schothorst J, Kankipati HN, Van Zeebroeck G, Rubio-Texeira M, Thevelein JM. Nutrient sensing and signaling in the yeast *Saccharomyces cerevisiae*. FEMS Microbiol Rev. 2014;38(2):254–99.